The 2010 IEEE/RSJ International Conference on
Intelligent Robots and Systems
October 18-22, 2010, Taipei, Taiwan

Forward kinematics of redundantly actuated, tendon-based robots

Joachim von Zitzewitz, Georg Rauter, Heike Vallery, André Morger and Robert Riener

Abstract— **The number of ropes for a fully constrained, tendon-based robot has to be larger than the actuated degrees of freedom since ropes only impose unidirectional constraints. This actuation redundancy implicates that more position information is available than would be required for the the determination of the end-effector pose. This leads to an optimization problem for the forward kinematics of the robot which has to be solved in real-time. Furthermore, the kinematics of tendon-based robots are often kept simple in existing systems by guiding the ropes through holes into the workspace. This facilitates the description of the rope vectors. However, this solution is not applicable for high-load applications, as friction would cause excessive non-linearities and wear. To solve the forward kinematics of tenon-based robots, we introduce a physics-based interpretation of the mentioned optimization problem. The robotic system is described as a damped oscillator whose resting position is equal to the optimal solution. As a major advantage over the known algorithms, this physics-based approach is quantifiable in terms of accuracy of the solution and number of iterations. Furthermore, the design and mathematical description of a deflection unit's geometry is presented. This deflection unit guides the rope smoothly into the workspace and its relevant influence on the kinematic equations can be compensated. The physics-based approach is experimentally evaluated on a tendon-based haptic interface, the r^3-system, and it is compared to the solutions using only the minimum set of sensor information.**

I. INTRODUCTION

Tendon-based robots (TBRs) are parallel manipulators whose end-effectors are supported by m separate cables. As other parallel robot types, TBRs have advantages over serial robots in terms of workload-to-weight ratio, stiffness, and accuracy.

Moreover, an increase of the workspace size hardly leads to an increase in inertia, which makes TBRs well-suited for large-scale haptic rendering.

Additionally to their minimal inertia, TBRs have another key difference to other parallel manipulators: The cables of TBRs only impose unidirectional constraints, since cables can only pull, not push. Therefore, the full control of n degrees of freedom requires $m > n$ ropes [1]; thus, TBRs are redundantly actuated and, as a consequence, redundant information of the end-effector pose is available.

The forward kinematics, i.e. the determination of the end-effector pose from the cable lengths, are an over-determined system of equations with m equations for n unknowns. Due to measurement inaccuracies, it is not possible to find a solution which satisfies all m equations at once; iterative optimization algorithms are usually employed to solve this problem at the cost of high computational load and/or uncertain calculation time [2]. When considering the position information of only n axes, the number of equations and unknowns are equal [2]. For this case, several approaches such as the Newton-Raphson method [3], [4] or interval analysis [5] have been presented in the literature. However, available position information is neglected.

A further challenge in forward kinematics of TBRs is to integrate the geometry of the deflection unit (DU) into the kinematic equations, as the geometry of the DUs introduce further non-linearities. A common work-around is to guide the ropes via holes, describable as a single point, into the workspace [2], [6], [7]. For high-load applications, this solution is not applicable; the high friction and, in consequence, the non-linearities in the applied force and the rope abrasion would negatively influence control performance and robot safety.

In this paper, we present a physics-based approach for the forward kinematics of redundantly actuated parallel robots. This approach allows a clear quantification of the computational load required to find a solution with a predefinable bound on accuracy. Furthermore, the mathematical description of a DU's geometry is explained. Due to this description, the influence of the DU on the forward kinematics can be minimized.

The physics-based forward kinematics (PBFK) are thereafter experimentally validated on the r^3-system. This robotic system serves as a large-scale, reconfigurable haptic interface embedded in a multi-modal Cave Automatic Virtual Environment (CAVE) [8]. The PBFK are compared to an analytical solution of the forward kinematics which incorporates only the minimal amount of position information.

II. FORWARD KINEMATICS OF REDUNDANTLY ACTUATED TBRS

A. Physics-based forward kinematics (PBFK)

In TBRs, the end-effector position and orientation can be derived from the supporting ropes' lengths $l_1 ... l_m$. All ropes are attached to the end-effector whose translation and

This work was was supported by local sources of the ETH Zurich

J. von Zitzewitz is with Sensory-Motor Systems (SMS) Lab, Institute of Robotics and Intelligent Systems (IRIS), ETH Zurich, 8092 Zurich, Switzerland zitzewitz@mavt.ethz.ch

G. Rauter is with Sensory-Motor Systems (SMS) Lab, Institute of Robotics and Intelligent Systems (IRIS), ETH Zurich, 8092 Zurich, Switzerland rauter@mavt.ethz.ch

H. Vallery is with Sensory-Motor Systems (SMS) Lab, Institute of Robotics and Intelligent Systems (IRIS), ETH Zurich, 8092 Zurich, Switzerland hvallery@ethz.ch

A. Morger is with Sensory-Motor Systems (SMS) Lab, Institute of Robotics and Intelligent Systems (IRIS), ETH Zurich, 8092 Zurich, Switzerland amorger@student.ethz.ch

R. Riener is with Sensory-Motor Systems (SMS) Lab, Institute of Robotics and Intelligent Systems (IRIS), ETH Zurich, 8092 Zurich, Switzerland, 8092 Zurich, Switzerland, and Medical Faculty, University of Zurich,8092 Zurich, Switzerland, riener@mavt.ethz.ch

orientation in a global coordinate system are described by the vector $\boldsymbol{x}$ and the rotation matrix $\mathbf{R}(\boldsymbol{\varphi})$, respectively. The vector $\boldsymbol{x}$ points to the origin of a local end-effector coordinate system, and the vector $\boldsymbol{\varphi}$ contains the three Euler angles describing the orientation of the end-effector. With $\boldsymbol{p}_i$ as the vector from the global origin to the deflection point where the i-th tendon is guided into the workspace, the length of the i-th rope would be:

$$l_i = \|\boldsymbol{p}_i - \boldsymbol{x} - \mathbf{R}(\boldsymbol{\varphi}) \cdot {}_{EE}\boldsymbol{v}_i\|. \tag{1}$$

with $i = 1..m$ and ${}_{EE}\boldsymbol{v}_i$ as the (constant) vector from the origin of the local end-effector coordinate system to the connection point of the rope, described in the local system (Fig. 1).

To obtain an estimate of the end-effector pose and orientation, the inverse problem needs to be solved, where rope lengths l_i are given and $\boldsymbol{x}$ and $\boldsymbol{\varphi}$ are to be found. Due to measurement errors, a single solution $[\boldsymbol{x}, \boldsymbol{\varphi}]$ which satisfies all equations cannot be found for an over-actuated system. An optimal estimate $[\hat{\boldsymbol{x}}_{opt}, \hat{\boldsymbol{\varphi}}_{opt}]$ for given (measured) rope lengths $\check{l}_i$ can be found by minimizing the following cost function:

$$V = \frac{1}{2} \sum_{i=1}^{m} \left(\|\widehat{\boldsymbol{s}}_i\| - \check{l}_i \right)^2 \tag{2}$$

with $\widehat{\boldsymbol{s}}_i$ as a function of the estimates $[\widehat{\boldsymbol{x}}, \widehat{\boldsymbol{\varphi}}]$

$$\widehat{\boldsymbol{s}}_i = \boldsymbol{p}_i - \widehat{\boldsymbol{x}} - \widehat{\mathbf{R}}(\widehat{\boldsymbol{\varphi}}) \cdot {}_{EE}\boldsymbol{v}_i \tag{3}$$

describing the approximated rope vector.

We now reinterpret the cost function V in (2) as the potential stored in m springs. These virtual springs are arranged in the same way as the ropes, and they are attached to a virtual rigid body with mass m and uniform inertia J around the chosen origin of the local coordinate system. The resting position of the virtual physical system corresponds to the best estimate $[\hat{\boldsymbol{x}}_{opt}, \hat{\boldsymbol{\varphi}}_{opt}]$ of the end-effector position and orientation.

Calculating the force exerted on the virtual body by the i-th spring with resting length $\check{l}_i$ as

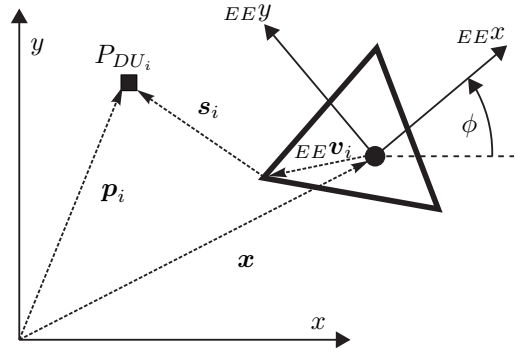

Fig. 1. Description of end-effector position and orientation in terms of rope lengths (body in 2D)

$$\boldsymbol{f}_i = c\boldsymbol{\zeta}_i \tag{4}$$

with c as the spring constant and

$$\boldsymbol{\zeta}_i = (\check{l}_i - \|\widehat{\boldsymbol{s}}_i\|) \frac{\widehat{\boldsymbol{s}}_i}{\|\widehat{\boldsymbol{s}}_i\|}, \tag{5}$$

the dynamics of the virtual rigid body are described by:

$$\begin{aligned} \ddot{\boldsymbol{x}} &= -\frac{c}{m} \sum_{i=1}^{m} \boldsymbol{\zeta}_i - \mathbf{D}_{xx}\dot{\boldsymbol{x}} - \mathbf{D}_{x\varphi}\dot{\boldsymbol{\varphi}} \\ \ddot{\boldsymbol{\varphi}} &= -\frac{c}{J} \sum_{i=1}^{m} \boldsymbol{\lambda}_i - \mathbf{D}_{\varphi x}\dot{\boldsymbol{x}} - \mathbf{D}_{\varphi\varphi}\dot{\boldsymbol{\varphi}}, \end{aligned} \tag{6}$$

with

$$\boldsymbol{\lambda}_i = (\mathbf{R}(\widehat{\boldsymbol{\varphi}}) \cdot {}_{EE}\boldsymbol{v}_i) \times \boldsymbol{\zeta}_i \tag{7}$$

with $\mathbf{D}_{xx}$,$\mathbf{D}_{x\varphi}$,$\mathbf{D}_{\varphi x}$, and $\mathbf{D}_{\varphi\varphi}$ as damping matrices.

This set of differential equations can be simulated numerically until the virtual physical system has settled in its resting position, where the minimum of the potential is located. The solution will tend toward this minimum if the values of c, m, $\mathbf{D}_x$, $\mathbf{D}_\varphi$ and J are positive/positive definite. The parameters of the oscillator and the integration method have to be chosen appropriately in order to warrant that the computation converges fast enough, i.e. within each time step of the real-time process. This choice is described in the following section.

B. Optimal parameter setting for the PBFK

To find appropriate parameters, the system is linearized around an initial position $[\boldsymbol{x}_0, \boldsymbol{\varphi}_0]$. The following substitutions are therefore introduced:

$$\mathbf{A} := \left[\begin{matrix} \frac{\partial \sum_{i=1}^{m} \boldsymbol{\zeta}_i}{\partial \boldsymbol{x}} & \frac{\partial \sum_{i=1}^{m} \boldsymbol{\zeta}_i}{\partial \boldsymbol{\varphi}} \\ \frac{\partial \sum_{i=1}^{m} \boldsymbol{\lambda}_i}{\partial \boldsymbol{x}} & \frac{\partial \sum_{i=1}^{m} \boldsymbol{\lambda}_i}{\partial \boldsymbol{\varphi}} \end{matrix} \right]_{[\boldsymbol{x}_0, \boldsymbol{\varphi}_0]} \tag{8}$$

$$\mathbf{B} := \begin{bmatrix} \mathbf{D}_{xx} & \mathbf{D}_{x\varphi} \\ \mathbf{D}_{\varphi x} & \mathbf{D}_{\varphi\varphi} \end{bmatrix} \tag{9}$$

$$\mathbf{M} := \begin{bmatrix} \frac{1}{m}\mathbf{E} & \mathbf{0} \\ \mathbf{0} & \frac{1}{J}\mathbf{E} \end{bmatrix} \tag{10}$$

$$\Delta\boldsymbol{\xi} := \begin{bmatrix} \Delta\boldsymbol{x} \\ \Delta\boldsymbol{\varphi} \end{bmatrix} \tag{11}$$

$$\tag{12}$$

and with $\mathbf{E}$ as a 3×3-identity matrix, and $\Delta\boldsymbol{x}$ and $\Delta\boldsymbol{\varphi}$ as the translational and rotatory deviation of the oscillator from the resting position of the linear system, respectively. Applying these substitutions, the linearization of (6) around the initial pose $[\boldsymbol{x}_0, \boldsymbol{\varphi}_0]$ can be rewritten as

$$\ddot{\boldsymbol{\xi}} \approx -c \cdot \mathbf{M}\mathbf{A}\Delta\boldsymbol{\xi} - \mathbf{B}\dot{\boldsymbol{\xi}}. \tag{13}$$

In a first step, the mass parameters m and J of this oscillator are chosen: The mass m can be set to $1\,\mathrm{kg}$ without

the loss of generality. The inertia J is used to scale the diagonal entries (a_4, a_5, a_6) in the lower half of $\mathbf{A}$ to the diagonal entries (a_1, a_2, a_3) in the upper half:

$$J = \frac{\min(|a_4|, |a_5|, |a_6|)}{\min(|a_1|, |a_2|, |a_3|)}. \quad (14)$$

Due to this scaling, the modes of the oscillator in translational and rotatory directions become similar.

The linear system defined in (13) can be transformed to a set of decoupled oscillators by using the transformation matrix $\mathbf{T}$, where $\mathbf{T}$ contains the eigenvectors of $\mathbf{MA}$. The transformed state vector $\boldsymbol{z}$ is then defined as:

$$\boldsymbol{z} := \mathbf{T}^{-1}\Delta\boldsymbol{\xi}, \quad (15)$$

such that the equations of motion of the decoupled oscillators are

$$\ddot{\boldsymbol{z}} \approx -c \cdot \mathbf{T}^{-1}\mathbf{MAT}\boldsymbol{z} - \mathbf{T}^{-1}\mathbf{BT}\dot{\boldsymbol{z}} = -c \cdot \tilde{\mathbf{A}}\boldsymbol{z} - \tilde{\mathbf{B}}\dot{\boldsymbol{z}}. \quad (16)$$

The matrix $\tilde{\mathbf{A}}$ is a diagonal matrix containing the eigenvalues of $\mathbf{MA}$.

The parameters of these decoupled oscillators are optimized in such way that the solution reaches a given accuracy after a pre-defined simulation time. The goal is to have adjusted stiffness and critical damping in all oscillators in order to approach the resting position as fast as necessary.

To obtain critical damping for each oscillator, the values $\tilde{b}_i$, the diagonal entries of $\tilde{\mathbf{B}}$, are chosen as functions of the stiffness:

$$\tilde{b}_i = 2\sqrt{c\tilde{a}_i}. \quad (17)$$

With this substitution, the slowest dynamics are determined by the smallest entry of $\tilde{\mathbf{A}}$, $\tilde{a}_{min}$, and the stiffness c:

$$\ddot{z}_{min} = -c\tilde{a}_{min}z_{min} - 2\sqrt{c\tilde{a}_{min}}\dot{z}_{min}. \quad (18)$$

With the initial conditions

$$z_{min}(0) = z_{0min} \quad (19)$$
$$\dot{z}_{min}(0) = 0, \quad (20)$$

the final position for this critically damped oscillator after a simulation time T is given as

$$z_{min}(T) = z_{0min}(1 + \sqrt{c\tilde{a}_{min}}T)e^{-\sqrt{c\tilde{a}_{min}}T}. \quad (21)$$

In order to quantify the required accuracy of the obtained result, a factor ε is introduced. This factor describes the maximal admissible ratio between the initial deviation z_{0min} and the final deviation obtained after T seconds $z_{min}(T)$:

$$z_{min}(T) \leq \varepsilon \cdot z_{0min}. \quad (22)$$

Inserting (22) into (21) gives

$$(1 + T\sqrt{c\tilde{a}_{min}})e^{-T\sqrt{c\tilde{a}_{min}}} \leq \varepsilon. \quad (23)$$

From this inequality, the minimal c can be calculated for given values of T and ε. Using this spring stiffness, all oscillators are guaranteed to reach the desired accuracy ε within the given time T.

As the matrix $\tilde{\mathbf{B}}$ and, thus, the generalized damping matrices $\mathbf{D}_x$ and $\mathbf{D}_\varphi$ as well as the parameters m, J, and c are now determined, the resting position $[\hat{\boldsymbol{x}}_{opt}, \hat{\boldsymbol{\varphi}}_{opt}]$ of the nonlinear oscillator (6) can be calculated numerically. The integration step size has to be chosen in accordance to the available calculation time of the control program. Despite the scaling of (14), the eigenvalues of $\mathbf{MA}$ can differ in magnitude. In order to deal with such a stiff system, an implicit integration method is advisable. The use of an implicit method is not a problem as the oscillator is only simulated, although embedded within each time step of the real-time process. Thus, the simulation of the oscillator is not restricted by causality constraints. The simulation step size should be small enough for the mode with the highest eigenvalue.

The initial position of the oscillator for the k-th sampling step $\boldsymbol{x}_k(0)$ and $\boldsymbol{\varphi_k}(0)$ can be interpolated from the estimated optimal poses from the two previous samples of the real-time process:

$$\boldsymbol{x}_k(0) = \boldsymbol{x}_{k-1}(T) + \frac{\boldsymbol{x}_{k-1}(T) - \boldsymbol{x}_{k-2}(T)}{T_s} \quad (24)$$
$$\boldsymbol{\varphi}_k(0) = \boldsymbol{\varphi}_{k-1}(T) + \frac{\boldsymbol{\varphi}_{k-1}(T) - \boldsymbol{\varphi}_{k-2}(T)}{T_s} \quad (25)$$

with T_s as the sampling time of the robot's control program. The initial velocities are set to zero in accordance with (20).

C. Integrating the geometry of the deflection unit into the forward kinematics

The major design criteria for the DUs of the r^3-system were (a) a proper guidance of the rope (prevention of rope derailing), (b) minimization of mechanical ware of the rope (small friction, sufficiently dimensioned deflection diameters), (c) no induction of oscillation on the rope (no pivoting DOFs), and (d) an influence on the forward kinematics which is either negligible or which can be compensated mathematically.

A deflection through a hole resulting in a single deflection point would fulfill the requirement (a), (c) and (d) while it does not meet requirement (b). Several design steps yielded a solution where the rope is first deflected between two larger pulleys and is then guided into the workspace between two rollers (Fig. 2).

For the integration of the geometry into the forward kinematics, we assume that the rope enters the workspace from a point C on a deflection line parallel to the roller axes (Fig. 3). The correct length l_{roller} of the rope part deflected around the roller (length between points C and E) depends on the roller radius r_2 and on the rope deflection angles α and β around the pulley and the roller, respectively.

Fig. 2. Deflection unit for a tendon-based robot

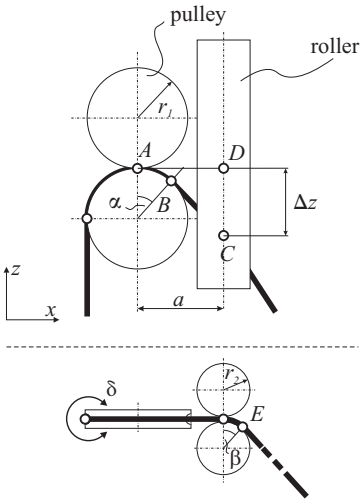

Fig. 3. Side and top view of the deflection unit

$$l_{roller} = \frac{r_2 \cdot \beta}{\cos\alpha} \tag{26}$$

The distance from the deflection unit to the end-effector is much larger than r_2. Hence, the length l_{roller} can be approximated under the assumption that the rope leads on a straight line from C to the end-effector. This approximated length l_{est} is

$$l_{est} = \frac{r_2 \cdot \sin\beta}{\cos\alpha}. \tag{27}$$

The error $e = l_{roller} - l_{est}$ due to the assumption that the rope leaves the DU at the point C and not at E decreases with the reduction of β and r_2. In our setup ($r_2 = 10\,\mathrm{mm}$), for the maximal deflection angles $\alpha = 70°$ and $\beta = 35°$, an error e of $6.9 \cdot 10^{-4}\,\mathrm{m}$ is obtained and, therefore, will be neglected.

A further advantage of a small angle β is a reduction of rope ware. Therefore, the DU can be rotated around an axis which is collinear with the rope coming from the motor, and can be fixed at an angle δ in order to minimize β for different applications.

Neglecting r_2 as described above, the rope length inside the deflection unit, l_{DU}, depends only on α. The change of l_{DU}, in our case over $3 \cdot 10^{-2}\,\mathrm{m}$, cannot be neglected for the kinematical calculations. It can be calculated as

$$l_{DU} = l_{AB} + l_{BC} \tag{28}$$

with

$$l_{AB} = r_1 \cdot \alpha \tag{29}$$

and

$$l_{BC} = \frac{a - r_1 \cdot \sin\alpha}{\cos\alpha}. \tag{30}$$

The length l_m is the measured rope length from A to the rope end inside the workspace, e.g. obtained from the motor encoder of the drive train. The rope length l inside the workspace can consequently be calculated as

$$l = l_m - l_{DU} \tag{31}$$

Also the position of the approximated deflection point C depends uniquely on α. The displacement Δz of C relative to the central point D is

$$\Delta z = -a \cdot \tan\alpha - r_1\left(1 - \frac{1}{\cos\alpha}\right) \tag{32}$$

The vector $\boldsymbol{\gamma}$ contains the angles which describe the orientation of the deflection unit in global space. With $\mathbf{R}_{DU}(\boldsymbol{\gamma})$ as the corresponding rotation matrix, the vector $\boldsymbol{p}$ to the deflection point can be calculated as

$$\boldsymbol{p} = \boldsymbol{x}_D + \mathbf{R}_{DU} \cdot (0\ 0\ \Delta z)^T \tag{33}$$

The angle α can be approximated from the position of the rope connection point on the end-effector $\boldsymbol{q} = [q_x, q_y, q_z]^T$ and $\boldsymbol{p} = [p_x, p_y, p_z]^T$. For a vertically mounted deflection unit (roller axes parallel to z-axis), α is

$$\alpha = \arctan\left(\frac{q_z - p_z}{\sqrt{(q_x - p_x)^2 + (q_y - p_y)^2}}\right). \tag{34}$$

with the z-axis being parallel to the roller axes.

The angle α can be calculated from $\boldsymbol{p}$ of the previous step without inducing a significant error; as a certain distance between the end-effector and the DUs is normally required in order to keep the rope forces within the given limits, the change of α between two sampling steps is small even for high end-effector velocities and especially for high sampling frequencies.

III. Experimental Validation on the R^3-System

A. The r^3-rowing application

An application of the r^3-system is a rowing simulator. In this simulator, five ropes are connected to a single point on the outer part of a cut oar (Fig. 4). The system is used as

Fig. 4. Rowing simulator with the r^3-system as a haptic interface

a 3D-haptic interface which can either render oar forces or provide haptic guidance to the user. The system runs at a sampling frequency of $4\,\mathrm{kHz}$.

B. Additional measurement equipment - optical tracking system

In order to evaluate the end-effector position obtained from the forward kinematics, an exact reference measurement was required. An optical tracking system (QTM, Qualisys AB, Gothenburg, Sweden) was used to measure the position of the end-effector point $\boldsymbol{x}_{opt}$. Furthermore, the tracking system was used to measure the position of the deflection units.

C. Comparison between PBFK and analytical approach

The approach of integrating all position information available into the forward kinematics, in our case the PBFK, is compared to the forward kinematics using only the minimal number of rope lengths l_i. Having a 3-DOF-application (point in space), three out of the available five rope lengths are theoretically sufficient to calculate $\boldsymbol{x}$. As all ropes are connected to one point, (1) is reduced to:

$$\|\boldsymbol{x} - \boldsymbol{p}_i\| = l_i. \tag{35}$$

with $i = 1..3$.

This system of equations can be solved analytically and was calculated for all 10 possible combinations of deflection units (1-2-3, 1-2-4, 1-2-5, 1-3-4,...).

For the comparison of the solutions of the physics-based and the analytical forward kinematics, the end-effector was moved randomly through the entire workspace by hand with the end-effector force being set to zero.

The parameters of the damped oscillator (6) were set to $\varepsilon = 1\,\%$ and $T = 1\,\mathrm{s}$ divided into 100 steps of $0.01\,\mathrm{s}$. As the system was not expected to be stiff, we used an explicit integration method for reasons of simplicity. An off-line calculation for $T_{offline} = 5T$ was used as a reference to evaluate how close the end-effector of the virtual oscillator came to its real rest-position.

The end-effector position calculated from the kinematics using the PBFK $\boldsymbol{x}_{PBFK}$ and the analytical approach $\boldsymbol{x}_{AFK}$ (j= 1..10) were finally compared to the reference measurement $\boldsymbol{x}_{opt}$ measured with the tracking system.

TABLE I

POSITIONS OF THE DEFLECTION UNITS AND THE RESIDUUM OF THE MEASUREMENT

	x (m)	y (m)	z (m)	res. (m)
DU 1	5.0405	0.2488	3.7707	0.0007
DU 2	3.0210	1.3159	0.4223	0.0014
DU 3	4.0041	6.6096	0.4249	0.00007
DU 4	5.0411	4.6775	0.4561	0.00042
DU 5	5.1202	6.7131	3.5572	0.00072

IV. RESULTS

A. Evaluation of the reference measurement

The central points D_i between the rollers of the deflection units were measured at the positions given in table (Table I).

The reference end-effector position $\boldsymbol{x}_{opt}$ was measured with a mean residual of $4 \cdot 10^{-4}\,\mathrm{m}$ (standard deviation $1.8 \cdot 10^{-4}\,\mathrm{m}$), values obtained from the software of the tracking system.

B. Evaluation of the PBFK

The resting position of the oscillator calculated online, $\boldsymbol{x}_k(T)$, deviated maximally $3\,\mu\mathrm{m}$ from the real resting position $\boldsymbol{x}_k(5T)$. The deviation from the resting position was $0.89\,\%$ (standard deviation of $0.48\,\%$) of the initial deviation $\|\boldsymbol{x}_k(5T) - \boldsymbol{x}_k(0)\|$. The distance between the oscillators end-effector and its resting position over time show that critical damping of the virtual oscillator could be reached with the presented parameter (Fig. 5).

The algorithm had a computation time of $48\,\mu\mathrm{s}$.

C. Comparison between PBFK and analytical approach

The comparison of the PBFK with the analytical forward kinematics incorporating the minimal number of ropes revealed considerable differences between these two approaches. The maximal error of the best combination of deflection points for the analytical approach (DU 1-2-4) was 5 times larger than the maximal error of the physics-based

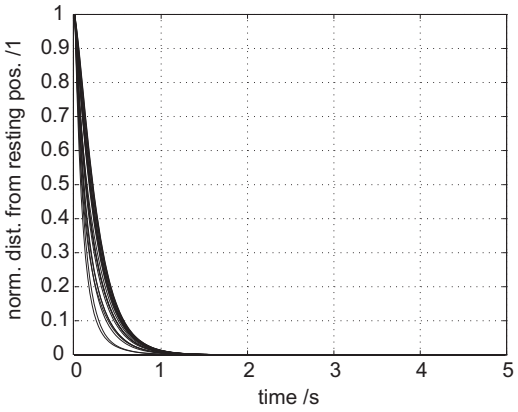

Fig. 5. Normalized distance of the virtual rigid body from its resting position calculated during 20 consecutive sampling step of the robot control program (online calculation of the oscillator movement until $t = T = 1\,\mathrm{s}$)

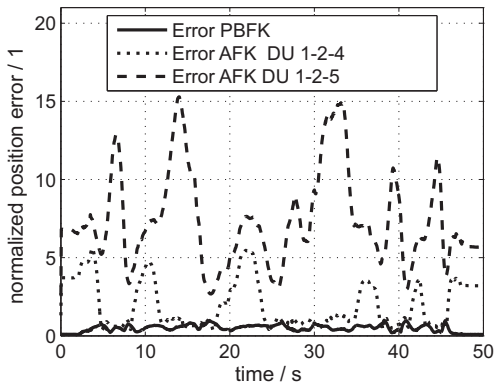

Fig. 6. Distance between reference position $\boldsymbol{x_{opt}}$ measured by the optical tracking system and end-effector position calculated from the robot forward kinematics (PBFK: physics-based forward kinematics, AFK: analytical forward kinematics)

approach. The maximal error of the worst combination (DU 1-2-5) deviated even by the factor of 15 (Fig. 6).

V. Discussion and Conclusion

In this paper, two major kinematic problems of TBRs were addressed: First, a physics-based approach for the forward kinematics of an over-actuated parallel robot was introduced. This approach is an alternative to the algorithms used to solve estimation problems in parallel robotics with redundant position information. The calculation time of these iterative algorithms for nonlinear optimization problems can normally not be predicted; hence, their use in real-time application is critical. Concerning the PBFK, the necessary number of simulation steps can be given until the virtual system reaches a region with a predefined maximal distance to its resting position (optimal position estimate of the real end-effector). The advantage of this approach (compared to e.g. gradient descent to minimize the cost function) is that it transfers the problem to a comprehensible mechanical analogon.

The second issue, the mathematical description of the DU geometry was an essential question at the very beginning of the design phase of the r^3-system. The solution described herein is mainly based on two approximations: first, the radius of the rollers is neglected. This makes the calculations of the rope deflection point easier; nevertheless, the calculation of the real deflection point on the roller would be feasible but more complicated. However, the influence of this neglect can be quantified when knowing the workspace limits of the end-effector and, derived from this, the maximal deflection angles of the rope. Secondly, the deflection angle α around the pulley is calculated from the approximated end-effector position obtained from the previous calculation step. Even for the most pessimistic assumption for our setup, we get a maximal error for l_i of $5 \cdot 10^{-4}\,\mathrm{m/s}$. The high sampling frequency of $4\,\mathrm{kHz}$ is of course favorable for this approach. In order to further decrease this error, a second iteration of the entire kinematic calculations could be performed.

Regarding the position accuracy, the approach incorporating all available sensor information, in our case the PBFK, shows a clear advantage over the analytical approach using the minimum set of position information, a result also reported in the literature [7], [9]. The considerable amelioration in the M^3 rowing simulator results from the double-redundant actuation. Concerning computational time, the analytical approach is of course superior due to the relatively simple system of equations for the 3D-case. However, general analytical solutions for more complex configuration with more DOFs are not available while the PBFK is still applicable.

Overall, the accuracy of the presented methods is by far sufficient for the r^3-system. Desired maximal translational position errors are in the range of approximately $1\,\mathrm{cm}$, as obtained with the PBFK for the rowing application. Regarding the dimensions of the r^3-system (rope lengths up to $10\,\mathrm{m}$ and frame dimensions of approximately $5 \times 6 \times 4\,\mathrm{m}$) and its use as a haptic interface for sport simulation, this value is acceptable. The errors induced by geometrical approximation as they occur in the used deflection unit are negligible compared e.g. to the influence of the nonlinear force-elongation relationship of the long, synthetic ropes. The presented approaches could be applied to over-actuated TBRs with any configuration and far higher demands on accuracy.

In case of the r^3-system, two further applications, a tennis simulator and a 6-DOF platform, are actually being developed.

References

[1] S. Kawamura, M. Ida, and T. Wada. Development of a virtual sports machine using a wire drive system - a trial of virtual tennis. In *Proc. IEEE/RSJ International Conference on Intelligent Robots and Systems*, pages 111–116, Pittsburgh, 1995.

[2] S. Fang. *Design, modeling and motion control of tendon-based parallel manipulators*. VDI Fortschritt-Bericht, 2005.

[3] C.C. Nguyen, S.S. Antrazi, J.Y. Park, and Z.L. Zhou. Trajectory planning and control of a stewart platform-based end-effector with passive compliance for part assembly. *Journal of intelligent & robotic systems*, 6(2-3):263–281, Dec 1992.

[4] J.P. Merlet. *Parallel Robots*. Kluwer Academic Publishers Norwell, MA, USA, 2002.

[5] J.P. Merlet. Solving the forward kinematics of a gough-type parallel manipulator with interval analysis. *The International Journal of Robotics Research*, 23(3):221, 2004.

[6] F. Faschinger, J. von Zitzewitz, and F. Pernkopf. Ein paralleler, 8-achsiger Seilroboter mit grossem Arbeitsraum als Handlingapplikation. In *Proc. Internationales Forum Mechatronik*, pages 218–228, Linz, Austria, 2006.

[7] Y. Cai, S. Wang, M. Ishii, and M. Sato. Position Measurement Improvement on a Force Display Device Using Tensed Strings. *IEICE Transactions on Information and Systems*, 79(6):792–798, 1996.

[8] J. von Zitzewitz, G. Rauter, R. Steiner, A. Brunschweiler, and R. Riener. A versatile wire robot concept as a haptic interface for sport simulation. In *Proceedings of the 2009 IEEE International Conference on Robotics and Automation (ICRA)*, pages 313–318, Kobe, Japan, 12-17 May 2009.

[9] F. Marquet, O. Company, S. Krut, and F. Pierrot. Enhancing parallel robots accuracy with redundant sensors. In *Proceedings of the 2002 IEEE International Conference on Robotics and Automation (ICRA)*, pages 4114–4119, Washington, DC, May 11-15 2002.